Journal of Nuclear Science and Technology

ISSN: 0022-3131 (Print) 1881-1248 (Online) Journal homepage: https://www.tandfonline.com/loi/tnst20

Using X-ray Energy Information in CT Measurement of a Phantom with an Al Region

Yuko MINAMI , Ryo IMAMURA , Ikuo KANNO , Masahiko OHTAKA , Makoto HASHIMOTO , Kuniaki ARA & Hideaki ONABE

To cite this article: Yuko MINAMI , Ryo IMAMURA , Ikuo KANNO , Masahiko OHTAKA , Makoto HASHIMOTO , Kuniaki ARA & Hideaki ONABE (2011) Using X-ray Energy Information in CT Measurement of a Phantom with an Al Region, Journal of Nuclear Science and Technology, 48:1, 108-112, DOI: 10.1080/18811248.2011.9711684

To link to this article: https://doi.org/10.1080/18811248.2011.9711684

Published online: 05 Jan 2012.

Journal of NUCLEAR SCIENCE and TECHNOLOGY, Vol. 48, No. 1, p. 108–112 (2011)

ARTICLE

Using X-ray Energy Information in CT Measurement of a Phantom with an Al Region

Yuko MINAMI[1,*], Ryo IMAMURA[1], Ikuo KANNO[1], Masahiko OHTAKA[2], Makoto HASHIMOTO[2], Kuniaki ARA[2] and Hideaki ONABE[3]

[1]*Graduate School of Engineering, Kyoto University, Sakyo, Kyoto 606-8501, Japan*
[2]*O-arai Research and Development Institute, Japan Atomic Energy Agency, Narita, O-arai, Ibaraki 311-1393, Japan*
[3]*Raytech Corporation, Yoto, Utsunomiya 321-0904, Japan*

(Received July 1, 2010 and accepted in revised form August 10, 2010)

X-ray computed tomography (CT) using X-ray energy information has been studied by the present authors on acrylic phantoms containing an iodine contrast medium. To observe a human body, however, it is necessary to consider the bone. In this paper, CT measurements were made on a phantom with regions of both iodine and aluminum, which was used as a substitute for the bone. A filtered back-projection method and a maximum likelihood-expectation maximization method were employed for image reconstruction.

KEYWORDS: X-ray, energy measurement, energy subtraction, photon detector, unfolding, contrast media, CT, transmission tomography, beam hardening

I. Introduction

X-ray computed tomography (CT) is one of the most powerful tools for the early detection of cancers. Iodine contrast media are occasionally employed to make cancers more visible in CT measurements. However, when the X-ray tube voltage is high or the subject through which X-rays pass is thick and dense, iodine contrast media are less visible when using the conventional method to measure X-rays as current. This phenomenon is called the beam hardening effect: after a polychromatic X-ray beam passes through a dense subject, the average energy of the X-ray beam increases since low-energy X-rays are preferentially absorbed.

The energy subtraction (ES) method was shown to be effective for avoiding the beam hardening effect.[1)] However, conventional measurement of X-ray energy is not suitable for practical CT because it is time-consuming. For a quick acquisition of the X-ray energy distribution, a new detector, which measures X-rays as current and gives the X-ray energy distribution, was invented by the present authors;[2)] this detector was named the transXend detector. The transXend detector consists of several segment detectors aligned along the direction of X-ray incidence. The X-ray energy distribution was estimated by an unfolding method.[3)] Then, CT images of the phantom with an iodine contrast medium were reconstructed by using the X-ray energy distribution.

In previous studies on X-ray CT with energy information,[1–3)] soft tissues (represented by the acrylic phantom) and blood vessels (iodine) were considered. However, the human body consists of not only soft tissues and blood vessels but also the bone. It is therefore necessary to consider the bone in simulating the observations of the human body.

In this paper, CT measurements were made on an acrylic phantom with regions of iodine and Al, which was used as a substitute for the bone. Filtered back-projection (FBP) and maximum likelihood-expectation maximization (ML-EM) methods were employed for image reconstruction.

II. TransXend Detector

1. Principle of TransXend Detector

A schematic view of the transXend detector is shown in **Fig. 1**. The detector consists of several segment detectors, which are aligned along the direction of the X-ray incidence. When polychromatic X-rays enter the detector, low-energy X-rays are absorbed in the forward segment detectors. On the other hand, high-energy X-rays partly penetrate the forward segment detectors and are absorbed by the backward segment detectors. X-rays absorbed by each segment detector are measured as current. The X-ray energy distribution is obtained from the measured current values using an unfolding method.

2. Unfolding Method

In this paper, six segment detectors were employed and the energy distribution of incident X-rays was divided into six energy ranges.

The relationship between the measured current value and the X-ray energy distribution is written as

*Corresponding author, E-mail: minami@nucleng.kyoto-u.ac.jp

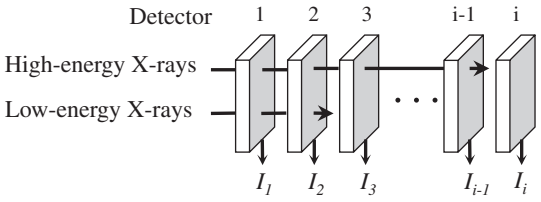

Fig. 1 Schematic view of the transXend detector

Table 1 Assigned energy ranges (keV)

Tube voltage	E_1	E_2	E_3	E_4	E_5	E_6
80 kV	20–27	27–33	33–39	39–50	50–65	65–80
100 kV	20–27	27–33	33–39	39–60	60–80	80–100
120 kV	20–27	27–33	33–39	39–60	60–90	90–120

$$\begin{pmatrix} I_1 \\ I_2 \\ \vdots \\ I_6 \end{pmatrix} = \begin{pmatrix} R_{1,1} & R_{1,2} & \cdots & R_{1,6} \\ R_{2,1} & R_{2,2} & & \vdots \\ \vdots & & \ddots & \\ R_{6,1} & \cdots & & R_{6,6} \end{pmatrix} \begin{pmatrix} Y_1 \\ Y_2 \\ \vdots \\ Y_6 \end{pmatrix}, \quad (1)$$

where I_i is the current value measured by each segment detector, Y_j is the incident X-ray events in the energy range, E_j, as indicated in **Table 1**, and $R_{i,j}$ is the response function of the ith channel detector in the energy range E_j. $R_{i,j}$ are calculated by using the SAND II code,[4] with initial guesses of $R_{i,j}$ calculated from the mass energy-absorption coefficients of Si. A detailed method for obtaining the response function is described in Ref. 2).

The X-ray energy distribution was calculated using the response function obtained for the acrylic thickness closest to the X-ray path length in the phantom. The calculation method is described in detail in Ref. 3).

III. Experiments

1. Experimental Setup

The experimental setup to obtain the response functions is shown in **Fig. 2**. The X-ray tube (TRIX-150S, Toreck Co., Ltd., Japan) had a built-in Al filter (2 mm thick) to absorb low-energy X-rays. A Pb collimator (5 mm diameter, 5 mm thick) and a La filter (100 μm thick) were attached to the X-ray tube. The La filter with a K-edge of 38.9 keV absorbed high-energy X-rays that were little influenced by the iodine contrast medium with a K-edge of 33.2 keV.

(1) X-ray Measurements for Response Function

A 7-mm-thick rectangular acrylic phantom was placed between the X-ray tube and the transXend detector. The phantom had four regions of iodine contrast medium with thicknesses of 15, 30, 45, and 60 μm. The transXend detector consisted of 6 Si(Li) segment detectors aligned along the direction of X-ray incidence. Each detector was $10 \times 10 \times 1\,\text{mm}^3$. Output signals were amplified with a 6-channel current preamplifier (IPA-6, Raytech Corp., Japan) and read by using timer counters with voltage-frequency converters (VFCT-8S4, Laboratory Equipments Corp., Japan). The current values for acrylic thicknesses of 7 to 67 mm were measured by adding 10-mm-thick acrylic slabs to the rectangular phantom. The position of the acrylic phantom on a precision stage was controlled by a computer to measure the current values for each iodine thickness. Measurements were done at a tube current of 2 mA and X-ray tube voltages of 80, 100, and 120 kV. Measured current values of each segment detector (subsequently referred to as a "channel") were fitted by exponential functions of the acrylic thickness for each iodine thicknesses. Response functions for acrylic thicknesses of 0 to 67 mm were acquired in 1 mm intervals.

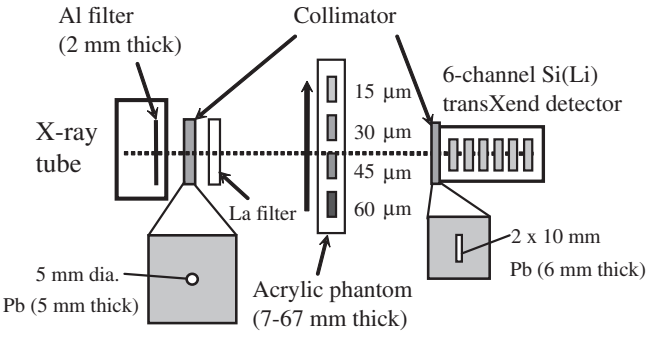

Fig. 2 Experimental setup

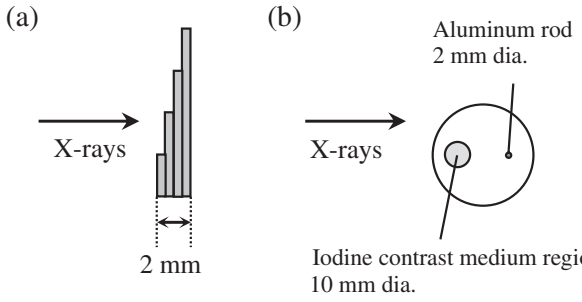

Fig. 3 (a) Al step wedge and (b) an acrylic phantom with iodine and Al regions for CT measurements

(2) Reference Measurements of X-ray Absorption by Aluminum

The acrylic phantom shown in Fig. 2 was replaced with an Al step wedge, which had thicknesses of 0.5, 1.0, 1.5, and 2.0 mm as shown in **Fig. 3**(a). Slabs of 10-mm-thick acrylic were incrementally added to the Al step wedge to measure current values for acrylic thicknesses ranging from 0 to 40 mm. The position of the Al step wedge was moved to measure current values for each Al thickness. Current values were used to analyze the Al absorption of X-rays.

(3) CT Measurements for Acrylic Phantom with Iodine and Aluminum

For CT measurements, the acrylic phantom shown in Fig. 2 was replaced with a 40-mm-diameter acrylic phantom, as shown in Fig. 3(b). The phantom had an iodine region with a diameter of 10 mm and an Al rod with a diameter of 2 mm. The iodine was 15 μm thick in a 10-

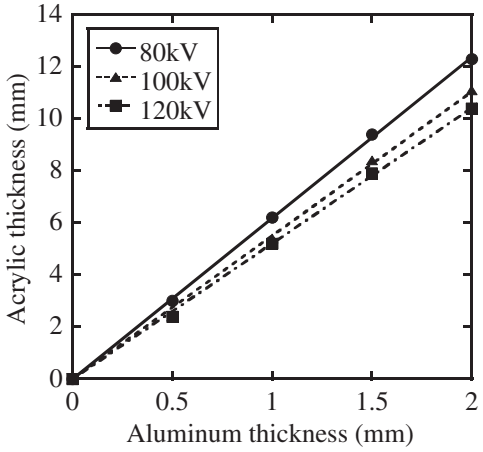

Fig. 4 Relationship between acrylic thickness and Al thickness in terms of X-ray absorption

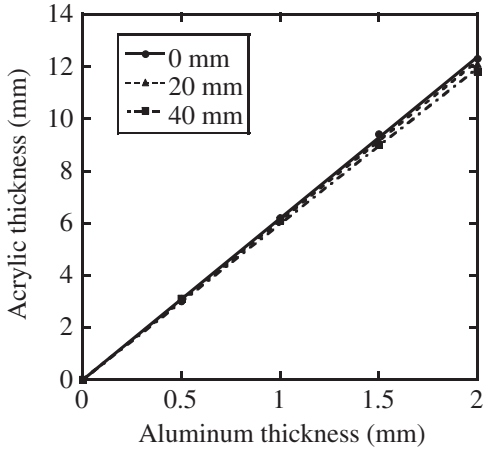

Fig. 5 Relationship between acrylic thickness and Al thickness in terms of X-ray absorption after passing through acrylic with thicknesses of 0, 20, and 40 mm. The X-ray tube voltage was 80 kV.

mm-thick water region. The phantom was translated for a distance of 44.4 mm (112 times at 0.4 mm increments) and then was rotated 10°. Translation and rotation were repeated 18 times until the phantom had been rotated 180° from the initial position.

2. Analysis of Aluminum X-ray Absorption

The X-ray attenuation coefficient curves of Al and acrylic have no discontinuous points such as a K-edge above 20 keV. Therefore, the Al thickness through which X-rays were transmitted can be converted to acrylic thickness. The difference between measured current values with each segment detector after X-rays passed through b-mm-thick Al, $I_{i,b}$, and w-mm-thick acrylic, $I_{i,w}$, is calculated as

$$\delta_{w,b} = \sqrt{\frac{1}{5}\sum_{i=1}^{6}(I_{i,b} - I_{i,w})^2}. \quad (2)$$

Equation (2) was calculated for each Al wedge thickness to build the relationship between acrylic thickness and Al thickness in terms of X-ray absorption. The b-mm-thick Al was regarded as the w-mm-thick acrylic in view of X-ray absorption when $\delta_{w,b}$ had the minimum value. When X-rays passed through only the Al step wedge, the relationship between the acrylic thickness and Al thickness to get the minimum value of $\delta_{w,b}$ is shown in **Fig. 4**. The converted acrylic thicknesses became smaller as the tube voltage increased because the X-ray attenuation coefficient of acrylic became relatively larger compared with that of Al as X-ray energy increased. The relationship between acrylic and Al thicknesses after X-ray transmission through acrylic thicknesses of 0, 20, and 40 mm at a tube voltage of 80 kV are shown in **Fig. 5**. The estimated acrylic thicknesses also became slightly smaller as the X-ray path length in the acrylic increased due to the beam hardening effect. The Al thickness was converted to the equivalent thickness of acrylic in view of X-ray absorption, using the results of Figs. 4 and 5 and taking into account of the beam hardening effect caused by the increases of acrylic thickness and the X-ray tube voltage.

IV. Results and Discussion

A current-based CT image was reconstructed using the sum of the current values measured by each segment detector. Acrylic and Al thicknesses, which X-rays passed through at each measured point, were obtained by a CT image reconstructed with current values.

1. Aluminum Thickness Calculated as Acrylic Thickness

The Al thickness was converted to the acrylic thickness and was added to the X-ray path length in the acrylic phantom. Energy-based and ES-based CT images were reconstructed using Y_3 and Y_2/Y_3, respectively. **Figure 6** shows the (a) current-based, (b) energy-based, and (c) ES-based CT images obtained with the FBP method where Al thickness was converted to acrylic thickness for tube voltages of 80, 100, and 120 kV. The number of streak artifacts was equal to the number of phantom rotations. If the number of rotations increases, the streak artifacts will become less obvious.[5] CT values at the center of the phantom are shown in **Fig. 7**. In current-based CT, the difference between the CT values in the acrylic region and the iodine region decreased as tube voltage increased due to the beam hardening effect, while the differences in CT values for those in both the energy-based and ES-based CT remained constant despite the change in tube voltage. In ES-based CT, CT values in the Al and iodine regions were positive and negative, respectively; the X-ray attenuation coefficient of iodine in the energy range E_3 was larger than that in the energy range E_2, while the attenuation coefficient of Al in the energy range E_3 was smaller than that in the energy range E_2. Thus, it was easy to distinguish Al from the iodine contrast medium in the ES-based CT where Al thickness was converted to acrylic thickness. The CT values in the Al region decreased as tube voltage increased in both the energy-based and ES-based CT, while the CT values of the iodine region stayed nearly the same. This phenomenon was caused by a decrease in acrylic thicknesses that corresponded to Al

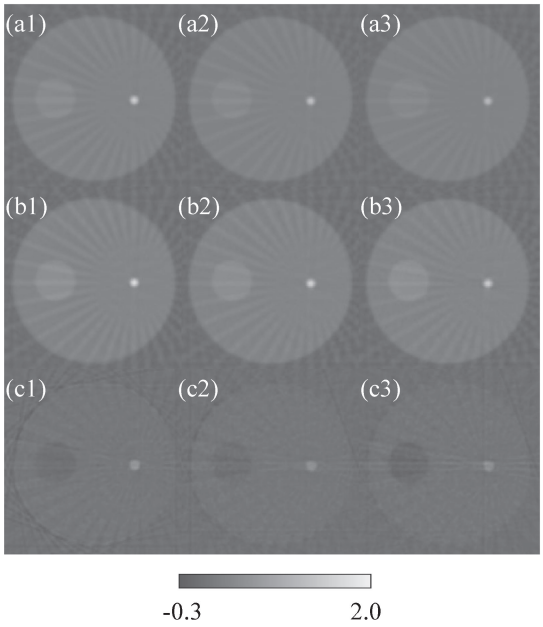

Fig. 6 (a) Current-based, (b) energy-based, and (c) ES-based CT images reconstructed with the FBP method. The X-ray tube voltages were 80, 100, and 120 kV, respectively, for images (1), (2), and (3).

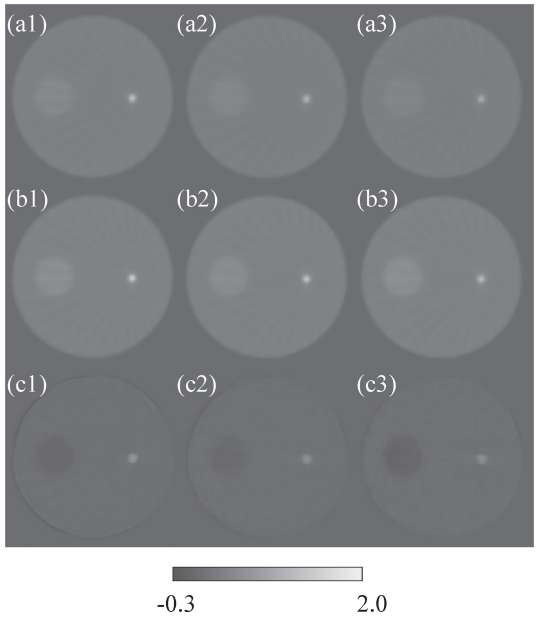

Fig. 8 (a) Current-based, (b) energy-based, and (c) ES-based CT images reconstructed with the ML-EM method

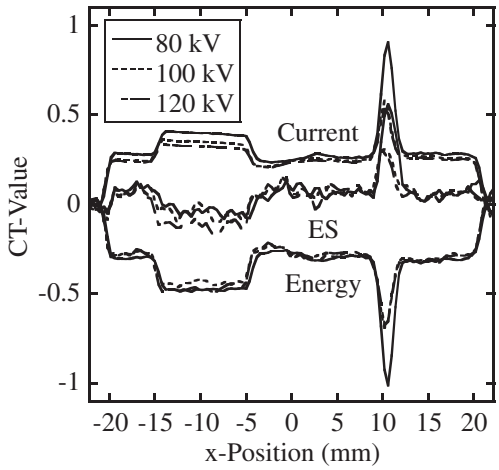

Fig. 7 CT values of the current-, energy-, and ES-based CT images shown in Fig. 6 (the energy CT values are multiplied by −1 for clarity).

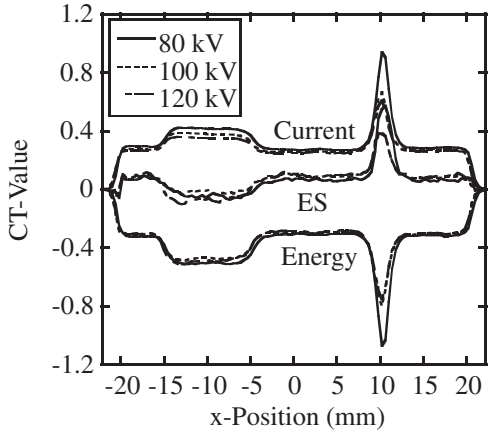

Fig. 9 CT values of the current-, energy-, and ES-based CT images shown in Fig. 8 (the energy CT values are multiplied by −1 for clarity).

thickness as tube voltage increased. The fluctuation of CT values in the energy-based CT was less than that in the ES-based CT. This is the advantage of energy-based CT, which requires less calculation.

In the FBP method, it is necessary to increase the number of rotations to reduce streak artifacts. However, that leads to a longer measurement time, resulting in an increase in exposure dose. Therefore, the ML-EM method, which is superior to the FBP method in terms of the removal of streak artifacts, is useful. With the ML-EM method, the (a) current-based, (b) energy-based, and (c) ES-based CT images were reconstructed at tube voltages of 80, 100, and 120 kV, as shown in **Fig. 8**. CT values at the center of the phantom are shown in **Fig. 9**. In comparison with Figs. 6 and 7, the CT images reconstructed with the ML-EM method had less streak artifacts and fewer fluctuations of the CT values than those reconstructed with the FBP method.

2. Aluminum Thickness Calculated as Iodine Thickness

Figure 10 shows the (a) energy-based and (b) ES-based CT images reconstructed with the FBP method where Al thickness was not converted to acrylic thickness. The X-ray energy distribution was obtained by choosing response functions according to the X-ray path length in the acrylic region. The CT values measured at the center of the phantom are shown in **Fig. 11**. The CT values in the Al region and iodine region were on the same side because the Al X-ray

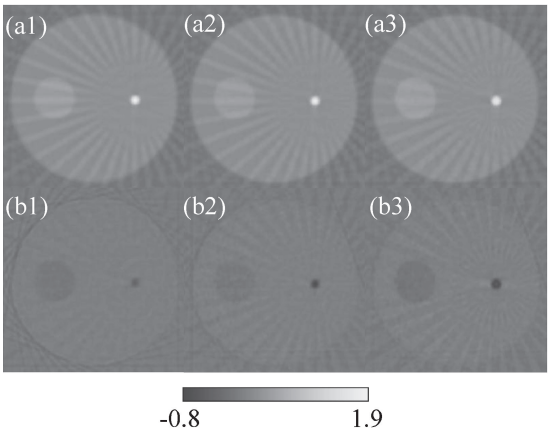

Fig. 10 (a) Energy-based and (b) ES-based CT images reconstructed with the FBP method where Al thickness was not converted to acrylic thickness. The X-ray tube voltages were 80, 100, and 120 kV, respectively, for images (1), (2), and (3).

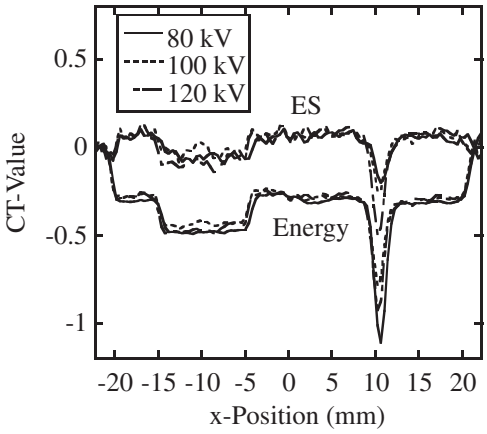

Fig. 11 CT values of the energy- and ES-based CT images shown in Fig. 10 (the energy CT values are multiplied by −1 for comparison with Fig. 7).

absorption was counted as the absorption by iodine. When CT images were reconstructed with the ML-EM method, the amounts of streak artifacts and fluctuations decreased as observed in Fig. 8.

V. Conclusion

In this paper, CT images of the acrylic phantom with both the iodine and Al regions were presented. When Al was regarded as having an equal thickness to acrylic in terms of X-ray absorption, the ES method had the advantage of being capable of distinguishing the Al region from the iodine region. Additionally, energy-based CT was better than the ES-based CT from the standpoint of fluctuations in the CT values. However, the fluctuations in the CT values were considerably reduced by using the ML-EM method.

Acknowledgments

The authors are deeply grateful to Prof. K. Watanabe, Nagoya University, for allowing them to use his CT reconstruction program. This work was supported by a Grant-in-Aid for Scientific Research from the Japan Society for the Promotion of Science and the Suzuken Memorial Foundation.

References

1) I. Kanno, A. Uesaka, S. Nomiya, H. Onabe, "Energy measurement of X-rays in computed tomography for detecting contrast media," *J. Nucl. Sci. Technol.*, **45**, 15–24 (2008).
2) I. Kanno, R. Imamura, K. Mikami, A. Uesaka, M. Hashimoto, M. Ohtaka, K. Ara, S. Nomiya, H. Onabe, "A current mode detector for unfolding X-ray energy distribution," *J. Nucl. Sci. Technol.*, **45**, 1165–1170 (2008).
3) R. Imamura, K. Mikami, Y. Minami, I. Kanno, M. Ohtaka, M. Hashimoto, K. Ara, H. Onabe, "Unfolding method with X-ray path length dependant response functions for computed tomography using X-ray energy information," *J. Nucl. Sci. Technol.*, **47**, 1075–1082 (2010).
4) W. McElroy, S. Berg, T. Crocket, G. Hawkins, *A Computer-Automated Iterative Method for Neutron Flux Spectra Determination by Foil Activation*, AFWL-TR-67-41 (1967).
5) P. P. Bruyant, J. Sau, J. J. Mallet, "Streak artifact reduction in filtered backprojection using a level line-based interpolation method," *J. Nucl. Med.*, **41**, 1913–1919 (2000).